ELSEVIER

Journal of South American Earth Sciences 18 (2004) 41–59

Journal of
South American
Earth Sciences

www.elsevier.com/locate/jsames

Paleomagnetism of Upper Triassic rocks in the Los Colorados hill section, Mendoza province, Argentina

Haroldo Vizán[a,*], Robert Ixer[b], Peter Turner[b], José María Cortés[a], Gerardo Cladera[c]

[a]*CONICET, Facultad de Ciencias Exactas y Naturales, Departamento de Ciencias Geológicas, Universidad de Buenos Aires (U.B.A.), Pabellón 2, Ciudad Universitaria, Buenos Aires C.P. 1428, Argentina*
[b]*School of Earth Sciences, The University of Birmingham, Edgbaston, Birmingham B15 2TT, UK*
[c]*CONICET, Museo Paleontológico Egidio Feruglio, Avenida Fontana 140, C.P. 9100 Trelew, Chubut, Argentina*

Received 1 May 2003; accepted 1 August 2004

Abstract

Different authors have highlighted a systematic disagreement between Late Carboniferous–Triassic paleomagnetic poles (PPs) for Gondwanaland and Laurasia when they are repositioned in a classical reconstruction prior to the breakup of Pangea A. This disagreement has been interpreted in geodynamic terms or as an evidence of non-dipole components of the geomagnetic field. Such analyses have been made using data on South American PPs published approximately 25 years ago and obtained using outdated methodologies. In this article, the authors present new Late Triassic paleomagnetic data from rocks that crop out in the Pre-Andean ranges (Precordillera) of Mendoza province (Argentina). Samples of different lithologies were taken from two limbs of a doubly plunging syncline, and several field tests of paleomagnetic stability were applied. The results indicate primary site mean directions that yield a PP with geographic coordinates and statistical parameters as follows: Lat. = 76°S, Lon. = 280°E, $N = 12$, $R = 11.63$, $\alpha_{95} = 8°$, $K = 30.2$. This PP agrees with mean PPs of Laurasia of similar ages in different models of Pangea A, indicating that the hypothesis of a dipolar paleomagnetic field could be valid for the Late Triassic.

Keywords: Argentina; Late Triassic; Paleomagnetism; Pangea; Precordillera

Resumen

Diferentes autores han señalado que existe un desajuste entre polos paleomagnéticos (PPs) de Gondwana y Laurasia para el lapso Carbonífero–Triásico, cuando los mismos son reconstruidos según un modelo clásico de Pangea A que se acepta como previo a la ruptura de este supercontinente. Este desajuste fue interpretado en términos geodinámicos, sugiriéndose reconstrucciones diferentes y previas a Pangea A, o como evidencia de componentes no dipolares del campo geomagnético. En todos los casos, los análisis se realizaron empleando bases de datos que incluyen PPs que fueron publicados hace aproximadamente 25 años atrás y que fueron obtenidos utilizando metodologías antiguas. En este trabajo se presentan nuevos datos paleomagnéticos triásicos tardíos de rocas que afloran en la Precordillera de la Provincia de Mendoza (Argentina). Para ello, se recolectaron muestras de litologías diferentes de dos limbos de un braquisinclinal. Diferentes pruebas de campo paleomagnéticas sugieren que las direcciones magnéticas aisladas en los sitios de muestreo, son primarias y con las mismas se obtuvo un PP cuyas coordenadas geográficas y parámetros estadísticos son: Lat. = 76°S, Lon. = 280°E, $N = 12$, $R = 11.63$, $\alpha_{95} = 8°$, y $K = 30.2$. Este PP se ajusta con otros PPs promedio de Laurasia de edades similares en diferentes modelos de Pangea A indicando que la hipótesis de un campo paleomagnético dipolar podría ser válida para el Triásico Tardío.

1. Introduction

Paleomagnetism is considered a powerful tool for testing continental reconstructions for time periods prior to

* Corresponding author. Tel.: +54 11 457 633 29; fax: +54 11 478 834 39.
E-mail address: haroldo@gl.fcen.uba.ar (H. Vizán).

0895-9811/$ - see front matter © 2004 Elsevier Ltd. All rights reserved.
doi:10.1016/j.jsames.2004.08.008

the generation of sea floor magnetic anomalies (e.g. Torsvik et al., 2001). However, the configuration of Pangea, the supercontinent where all the continents were assembled together from the Late Carboniferous to the Middle Jurassic, remains a matter of much discussion in the paleomagnetic community (Van der Voo, 1993; Muttoni et al., 1996; Torcq et al., 1997; Van der Voo and Torsvik, 2001). Different authors have pointed out a systematic disagreement between Late Carboniferous–Triassic paleomagnetic poles (PPs) of Gondwana and Laurasia when they are repositioned in a classical Pangea A configuration, accepted as the configuration at the time of its breakup. Some paleomagnetists have interpreted this disagreement in geodynamic terms and proposed different models as possible reconstructions that precede Pangea A (Van der Voo and French, 1974; Irving, 1977; Smith et al., 1981; Smith and Livermore, 1991); different geological arguments appear to support each model (Arthaud and Matte, 1977; Hallam, 1983; Ricou, 1994). However, Rochette and Vandamme (2001) note that the apparent difference between the PPs of the two supercontinents could be due to the paleomagnetic inclination error of sediments and Smith (1999) has suggested that the 'Pangaea problem' is probably because many Gondwana poles for the period 340–200 Ma have been remagnetised. Other researchers have related the misfit of the PPs to non-dipole components of the geomagnetic field (Briden et al., 1970; Van der Voo and Torsvik, 2001). Smith (1997), however, suggested that it is not necessary to postulate that the Earth had marked non-dipole components, and Kent and Olsen (2000) demonstrate a strong correlation between magnetic paleolatitudes and lithofacies distributions, in support of the notion of a dipolar field. In contrast, Geuna and Ecostegui (2003) recently have suggested that the misfit in some Late Paleozoic PPs of Argentina is due to local tectonic rotation of the sampling areas around a vertical axis.

In general, the misfit of PPs has been analyzed with a database that includes data from South America and Africa published 25 years ago and obtained using old methodologies. Specifically, many works used the blanket demagnetizations method; orthogonal diagrams and remagnetization circles were not used to define magnetic components; no field tests were performed to constrain the ages of the magnetization and the minerals that carry the remanences were not identified through rock magnetism or petrographic studies. In addition, one of the most important reliability criteria for a PP is the accurate age determination of the analyzed geological unit (Valencio, 1980; Van der Voo, 1993). Thus, a definitive answer for the misfit of PPs cannot be found until new, well-dated, reliable paleomagnetic data from South America improve the database.

With this idea in mind, we present new paleomagnetic results obtained from the Triassic rocks of the Portezuelo Bayo and Los Colorados Formations from Mendoza Province (Argentina). Several field tests indicate that the characteristic remanent magnetizations (ChRMs) may have an age close to that of the analyzed rocks that cover a time span between the mid–Late Triassic and the latest Triassic or Early Jurassic. The obtained PP fits very well with those of Laurasia, with equivalent ages in models of Pangea A that are geologically and tectonically supported. This fit is in agreement with the assumption that the average ancient geomagnetic field represents a geocentric dipole at the time that the rocks recorded the ChRMs.

2. Geological setting and sampling

The selected outcrops are located in Paramillo de Uspallata (32°25′S, 69°15′) in the Precordillera (Pre-Andean ranges) of Mendoza (Fig. 1a and b). The main sampled section is located on the eastern slope of the hill Los Colorados, where the Portezuelo Bayo and Los Colorados Formations (Harrington, 1971; Cortés et al., 1997) crop out. Both geological units have been correlated with the Río Blanco Formation (Fossa-Mancini, 1937; Rolleri and Criado Roqué, 1968; Harrington, 1971), which is the regional name given to the upper unit of the Uspallata Group (Stipanicic, 1969). The Group forms part of the rift infill of the Cuyana Basin (Ramos and Kay, 1991), whose stratigraphy has been studied by several authors mainly because of its potential hydrocarbon resources (Stipanicic, 1983; Strelkov and Alvarez, 1984; Kokogian and Mancilla, 1989; Kokogian et al., 1993, 2000).

Sixty-eight hand or block paleomagnetic samples (nine sites) from the Triassic section of Los Colorados hill (Fig. 1c) and 19 samples (three sites) from a complementary section, exposed a few kilometers south, were collected. Orientation was accomplished by both magnetic and solar compasses. Both sections belong to a brachisyncline; the northern sector has an axis plunging 9° to the south (Azimuth 198°) and the southern sector has an axis plunging 10° to the north (Azimuth 351°). In contrast, the beds of the northern sector (Los Colorados) dip to the west (strike: 171°, dip: 21°), and the beds of the southern sector (the complementary) dip to the east (strike: 324°, dip: 68° and strike: 335°, dip: 42°). According to regional geologic considerations (Cortés et al., 1997), the brachisyncline could have developed during a single phase of deformation during Andean tectonics.

The stratigraphy of the section of the Los Colorados hill (Fig. 1c) has been studied in detail by Harrington (1971), Massabie et al. (1985), and Kokogian and Boggetti (1987). Close to the top of the section, the sedimentary rocks are interbeded with volcanic units that have been interpreted in different ways. We agree with Kokogian and Boggetti (1987), who believe the rock to be an upper Mesozoic basaltic lava flow (our paleomagnetic site S1) rather than a sill emplaced between Triassic beds (Harrington, 1971; Massabie et al., 1985). A peperite lies beneath the lava flow, which indicates that the lava flow was contemporaneous with the Mesozoic sedimentary beds (e.g. Busby-Spera and

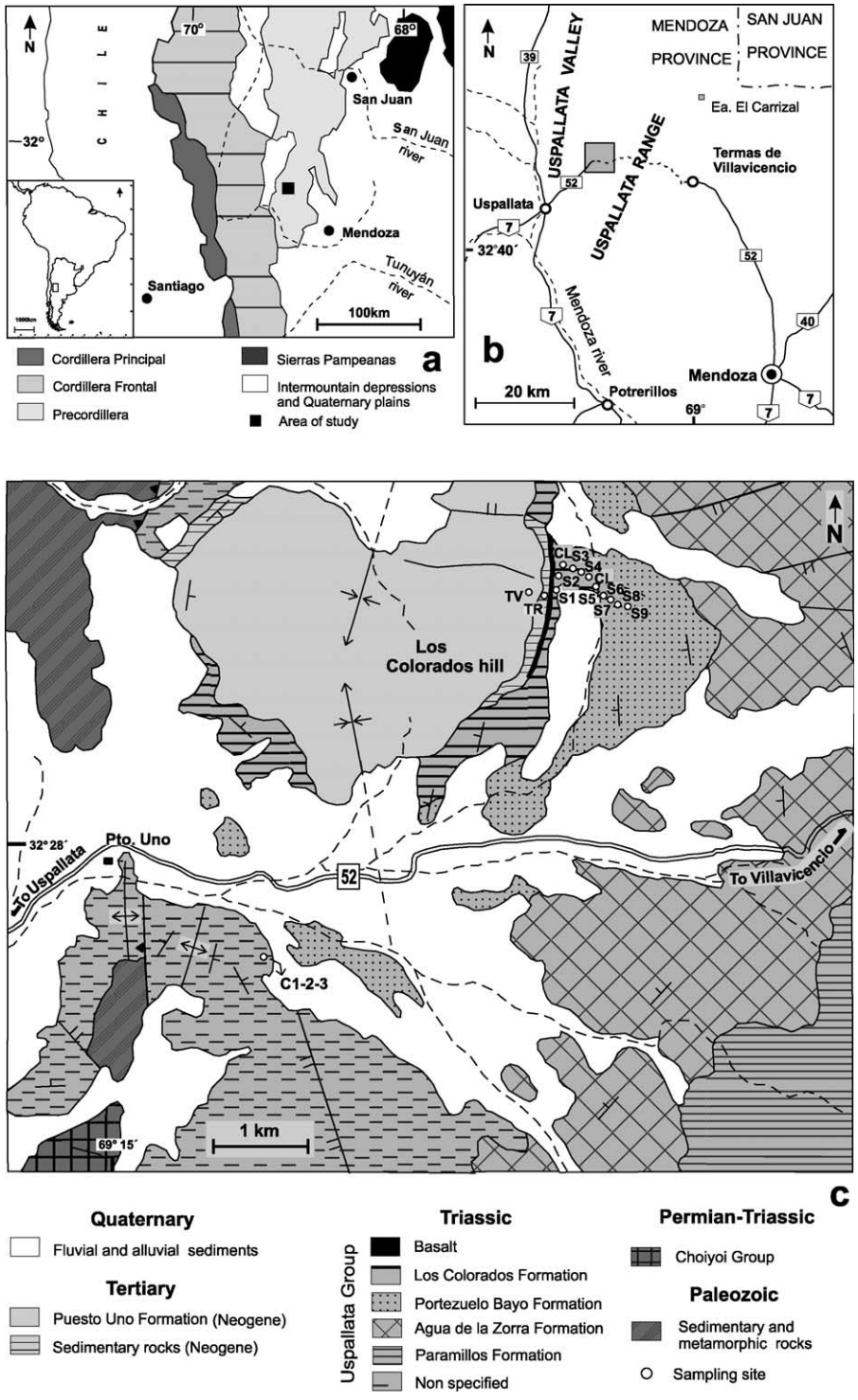

Fig. 1. (a) Location of the study area in relation with main morphotectonic units of western Argentina. (b) Sketch map with the main routes of the sampling locality (gray square). (c) Geological map of the sampling area with paleomagnetic sites (S: Los Colorados section, C: complementary section, TV: Miocene volcanic rocks, TR: Miocene red beds, CL: clasts for the conglomerate tests). Based on Cortés et al. (1997).

White, 1987). On the basis of taxa associations, Spalletti et al. (1999) assign a late Neo-Triassic age to the Río Blanco Formation. In the Los Colorados section, fossil plants support this age (Harrington, 1971; Massabie et al., 1985; Artabe et al., 1999). Kokogian and Boggetti (1987), on the basis of stratigraphic correlations with other sections, indicate that the age of the top of the section is Early Jurassic (Hettangian).

Within the Los Colorados section, sampling included paleomagnetic sites on the tuff and tuffaceous sandstones of the Portezuelo Bayo Formation and paleomagnetic sites in the red beds and the basaltic lava flow and its underlying

peperite. To perform paleomagnetic stability tests, samples from 29 clasts were taken from two conglomerates of the Los Colorados Formation and at two sites in the Miocene rocks that form the upper part of the section (Fig. 1c). The latter sites were in the Puesto Uno Formation that Cortés et al. (1997) suggest rests with a low-angle discordance on the Los Colorados Formation. The Puesto Uno Formation includes sedimentary rocks interbedded with andesites that dominate the center of the hill and form the core of a volcano (Massabie et al., 1985). Two radiometric ages of 24 ± 2 and 19 ± 2 Ma (Massabie et al., 1985) indicate a Miocene age for this volcano. Samples from one paleomagnetic site in the andesites and one from the interbedded sedimentary rocks were collected (sites TV and TM in Fig. 1c).

Sampling in the complementary section concentrated on a basaltic lava flow and tuffs that Cortés et al. (1997) suggest are Triassic in age, though their stratigraphic position is still not well-defined. The section could belong to Río Blanco Formation or to the Agua de la Zorra Formation (Harrington, 1971), which is correlated with the Potrerillos and Cacheuta Formations (Fossa-Mancini, 1937; Harrington, 1971). Spalletti et al. (1999) assign a late Middle–early Late Triassic age to these units.

Thus, within both the Los Colorados hill and the complementary sections, the sampled rocks are Mesozoic and have ages that range from the late Middle Triassic to the late Late Triassic or Earliest Jurassic (Hettangian).

3. Experimental procedure

3.1. General methodology

One to five specimens of 2.5 cm diameter and 2.2 cm length were cut from each block sample. Natural Remanent Magnetizations (NRM) before and after demagnetizations were determined using a JR5 A and a DIGICO magnetometer at the Paleomagnetic Laboratory of the University of Birmingham (UK). The stability of the NRM was tested by progressive thermal or alternating field (AF) demagnetization. A mixed AF to 95 mT and then thermal demagnetization from 100 °C was sometimes used for specimens of the volcanic rocks and the peperite. During thermal cleaning, the bulk susceptibility was checked after each demagnetization step to monitor the occurrence of chemical changes induced by heating. In addition, isothermal remanent magnetizations (IRM) and, in some cases, stepwise thermal demagnetization of three IRM of different fields applied in three perpendicular axes (Lowrie, 1990) were carried out to identify the magnetic carriers of the samples. Petrographic analyses of thin and polished sections of rocks were also used to determine the magnetic carriers.

Different sorts of demagnetization behaviours were observed in different lithologies. They were grouped according to their precision to define the ChRMs and the methodologies used to calculate the site mean directions.

3.2. Cerro Los Colorados section

3.2.1. Basaltic lava flow and its associated peperite

The lava flow is highly altered, vesicular olivine basalt. Thin section petrography reveals very fine-grained skeletal FeTiO minerals, many of which display a feather-like texture. They are highly altered and replaced by abundant, fine-grained (1–5 μm diameter) haematite and TiO_2 mineral intergrowths or locally by a 10–40 μm diameter, euhedral, zoned grey/grey brown, anisotropic phase with strong, red, internal reflections. Later generations of haematite are associated with calcite infilling vesicles.

The IRM acquisition of this rock (Fig. 2a) shows a sharp rise of magnetization in magnetic fields (H) at less than 200 mT, followed by gradual acquisition of additional IRM in stronger H. The backfield shows a remanent coercive force (H_{cr}) around 180 mT. The IRM analysis is in agreement with the petrographic analysis and the blocking temperatures of this rock (Fig. 2b–d), which indicates that haematite and a ferrimagnetic mineral (magnetite?) were the carriers of the remanence.

The NRM bulk intensities range between 0.2 and 0.05 A m^{-1} and its susceptibility is approximately 150×10^{-6} SI. Stepwise AF cleaning was not enough to remove the NRM completely (Fig. 2b). A mixed AF/thermal cleaning revealed that similar components are carried by the different magnetic minerals. During the thermal cleaning, significant changes in the susceptibility without any change in the direction of the remanence were observed (Fig. 2c and d). We interpret this to mean that during the heating, new magnetic minerals were generated but did not record any new component because of the absence of any ambient magnetic field (the thermal demagnetizer was virtually field-free), and the original remanence was not disturbed.

The ChRM of each specimen was determined by applying a least squares line fitt (Kirschuink, 1980). All specimens showed very reliable behaviour, with well-defined upward magnetic components (MAD value $\leq 5°$) directed to the NNW with medium inclination.

The peperite from below the lava flow comprises alternating layers of claystone and very fine-grained sandstone with relatively large and angular peperites of vesicular lava clasts inserted in both layers. In the lava peperites, a 20–100 μm diameter, brown, zoned, equant phase enclosed within thin, 1–5 μm haematite rims, is poorly characterized. Because some grains are isotropic and others strongly anisotropic, there may be more than one phase present including possible magnetite, maghaematite, and TiO_2 minerals. Haematite replacing FeTiO minerals is also present.

The analysis of the IRM curves and the H_{cr} of about 100 mT are in agreement with the petrographic analysis and the blocking temperatures observed in the samples of

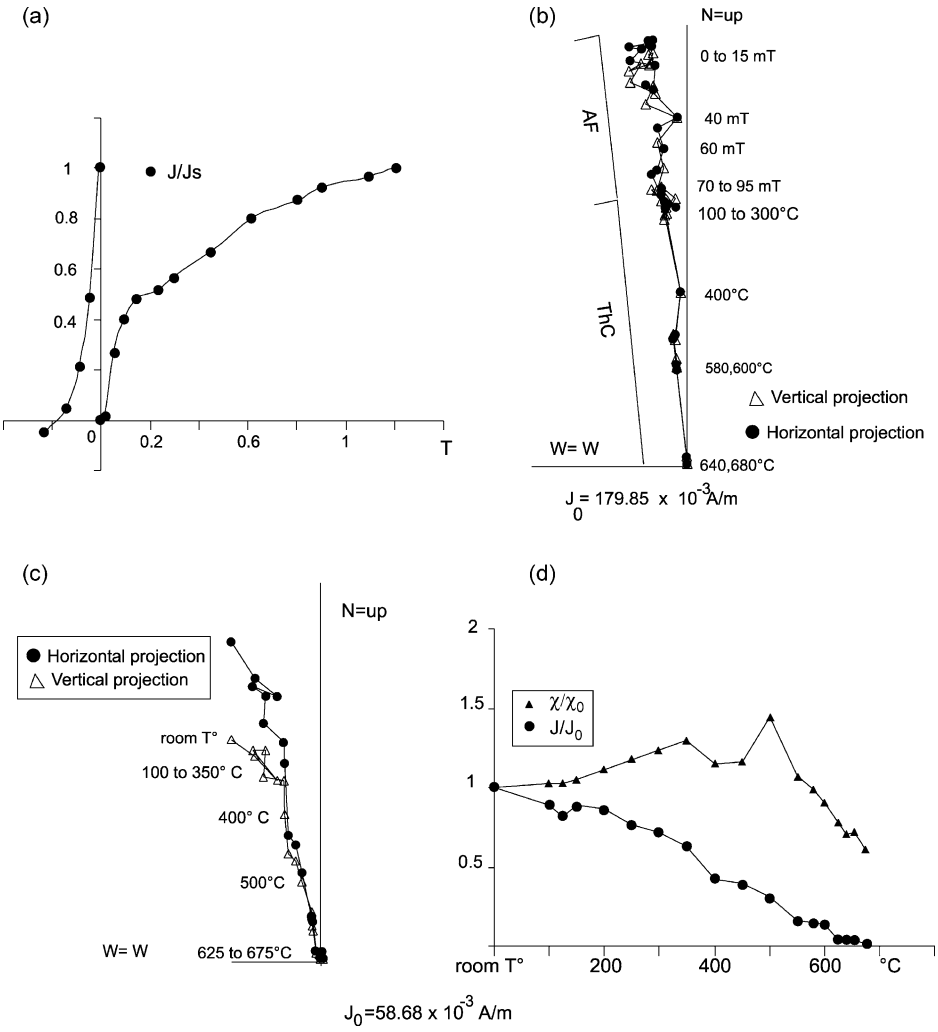

Fig. 2. Basaltic lava flow. (a) IRM acquisition curve and backfield, (b and c) orthogonal plot of demagnetization of NRM with open and closed symbols plotted, respectively, on the vertical and horizontal axes, in geographic coordinates; (b) mixed AF/thermal demagnetization, (c) thermal demagnetization, (d) normalized intensity decay after each thermal steps of demagnetization and bulk susceptibility evolution with increasing temperatures.

the peperite (Fig. 3b–d), which indicates that a ferrimagnetic mineral (magnetite?) and haematite are both carriers of the magnetic remanences. The NRM bulk intensities of the peperite range between 0.12 and 0.01 A m^{-1}, with an initial susceptibility of approximately 200×10^{-6} SI. As in the basaltic lava flow, a mixed AF/thermal demagnetization reveals that similar components are carried by different magnetic minerals (Fig. 3b). During thermal demagnetization, there are again significant changes in the susceptibility without any appreciable change in the magnetic directions (Fig. 3c and d). All the specimens of the peperite show very well-defined ChRMs (MAD value $\leq 5°$) similar to those obtained in the lava flow from just above it. We conclude that the same component was recorded at the same time (during the cooling of the lava flow) in both rocks. Fisher's (1953) statistics were used to calculate a mean direction for a single site composed of samples of the lava flow and peperite.

3.2.2. Epiclastic sedimentary rocks

The epiclastic sedimentary rocks of the Los Colorados section are arkosic siltstone/fine-grained sandstones and litharenites. In both rock types, reddened fine clay locally forms a matrix to the clastic component. Opaque minerals are uncommon in these sedimentary rocks. In the arkosic siltstone/fine-grained sandstones, they are dominated by haematite and fine-grained haematite–TiO_2 minerals that have replaced the original magnetite and magnetite–ilmenite intergrowths. Locally, relict 2–5 μm diameter magnetite is present in haematite. In the litharenites, opaques mainly constitute TiO_2 phases with lesser amounts of haematite. Most of the opaque component is present as inclusions in discrete quartz/feldespar grains or acid volcanic rock clasts that carry trace amounts of 5 μm diameter pyrrhotite, haematite, intergrowths of magnetite–ilmenite and limonite after sulphides.

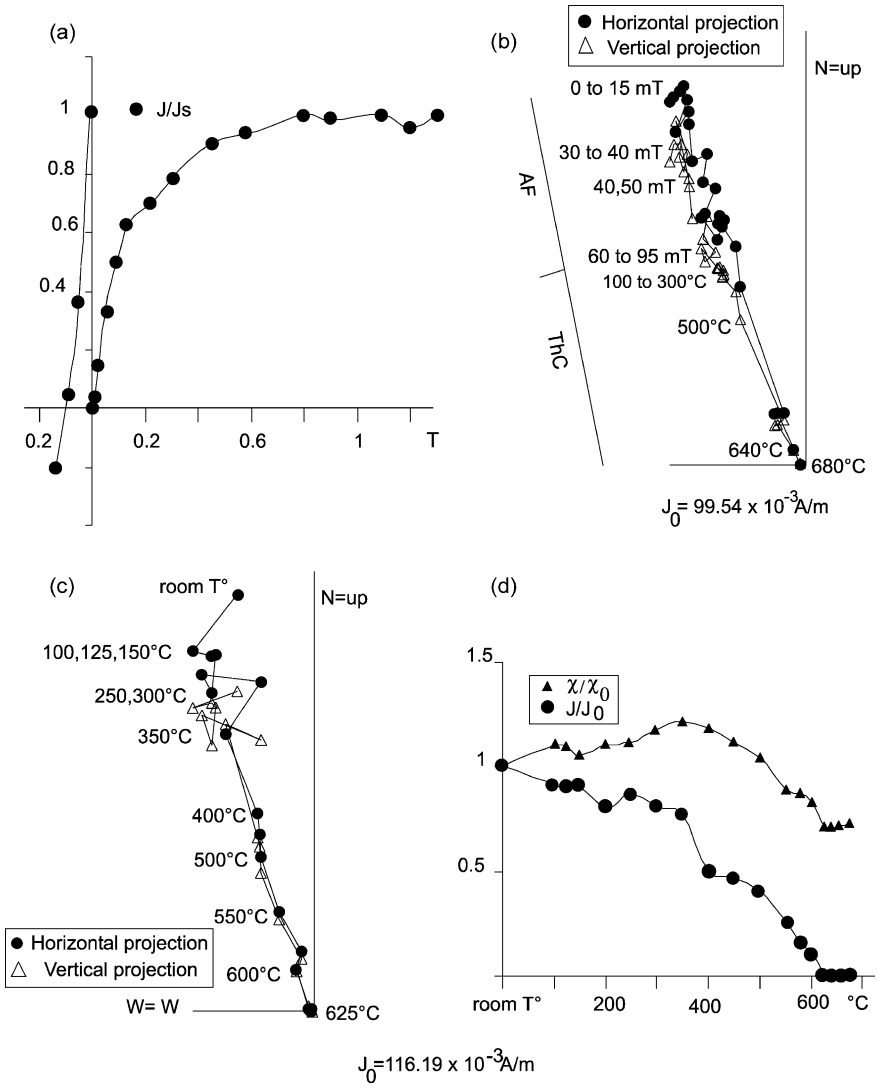

Fig. 3. Peperite. (a) IRM acquisition curve and backfield. (b and c) Orthogonal plot of demagnetization of NRM, symbols and reference as in Fig. 2; (b) mixed AF/thermal demagnetization, (c) thermal demagnetization. (d) Normalized intensity decay after each thermal step of demagnetization and bulk susceptibility evolution with increasing temperatures.

In Fig. 4, we show that the remanence of LC12 (H_{cr} of ~235 mT) is dominated by haematite, in agreement with the petrographic analysis and the blocking temperatures (Fig. 4c). In the case of LC15, the sharp rise at low values of H during the acquisition of IRM, suggest that a ferrimagnetic mineral is one of the carriers, and the value of H_{cr} (~115 mT) indicates that haematite also could be one of the carriers, as confirmed by applying Lowrie's (1990) method (Fig. 4b). The NRM bulk intensities of the epiclastic sedimentary rocks range between 0.002 and 0.0005 A m^{-1} and their initial susceptibilities are $\leq 25 \times 10^{-6}$ SI. We applied only thermal demagnetizations to these rocks and observe different magnetic behaviours according to the overlap of the coercivity spectra of their magnetic components. Fig. 4c represents those samples in which the magnetic components have a minimal degree of overlap in their blocking temperature spectra, and whose ChRM can be determined by applying least squares line fitting (MAD values $\leq 12°$) at steps higher than 200 °C. The ChRMs of these samples are directed upward with medium inclination to the NNW, similar to those of the site formed by the basaltic lava flow and the peperite.

Other samples show significant overlap in the blocking temperature spectra of their components, and the method previously applied fails to isolate a ChRM. In these cases, we display the data stereographically to analyze the great circle paths that fit best. Fig. 4d is an example of magnetic behaviour in which two great circle paths can be recognized; it shows the demagnetization plot for the sample and the corresponding vector differences for great circles when more than two vectors are involved (Hoffman and Day, 1978). In this case, the NRM is composed of three magnetic components, and the great circle defined by the highest temperature steps (580–675 °C) has a direction with NW–SE declination, which may correspond to the direction determined by least square analysis (Fig. 4c).

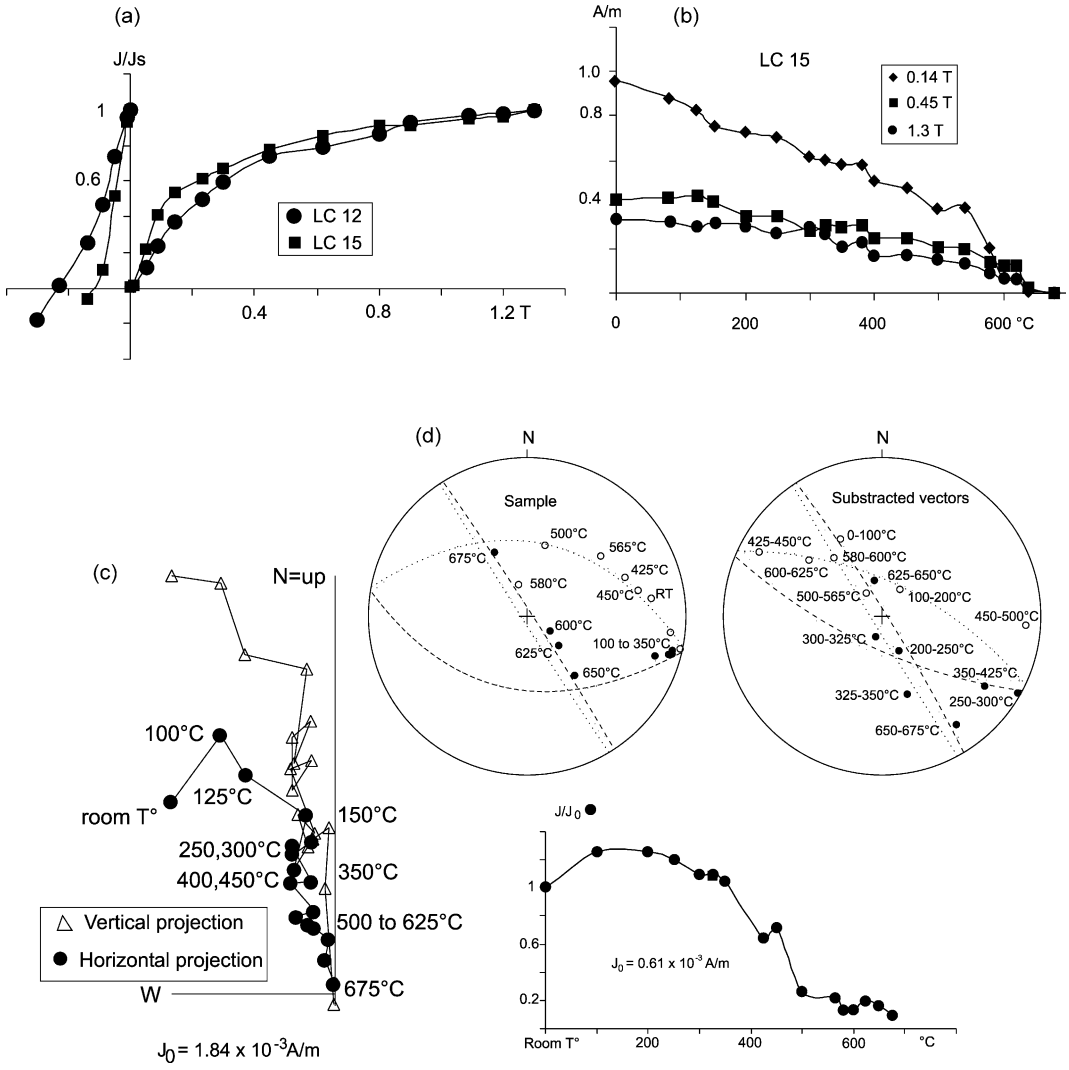

Fig. 4. Epiclastic rocks. (a) IRM acquisition curve and backfield of two representative samples (LC 12 and LC 15). (b) Thermal demagnetization of three IRM of different forces (1.3, 0.45 and 0.14 T) applied successively to each of three perpendicular axes of LC 15. (c) Orthogonal plot of thermal demagnetization of NRM of a representative sample; symbols and references as in Fig. 2. (d) Stereonet plot of resultant vectors after thermal cleaning of a representative sample (left) and difference vectors of the same sample (right). In both diagrams, open/closed circles indicate upward/downward pointing; below the stereonets: normalized intensity decay after each thermal steps of demagnetization.

3.2.3. Tuffs

The tuffs sampled in the Los Colorados section mainly comprise glass sherds and quartz crystals. Small needles of haematite (less than a half micron) are included in some of the shards. Opaque minerals are very uncommon, though clasts of maghemite of approximately 40 μm and haematite of approximately 20 μm diameter were observed in reflected light.

The acquisition of IRM and the backfield of these tuffs reveal different carriers of the magnetic remanence (Fig. 5a). In some samples the remanence is dominated by ferrrimagnetic minerals (H_{cr} of ~65 mT) (PB7 in Fig. 5a) as confirmed by applying Lowrie's (1990) method (Fig. 5b). Goethite is another remanence carrier in this sample (the higher axis shows blocking temperatures ~150°). In other samples, IRM experiments reveal haematite and/or goethite as carriers of the remanence (H_{cr} of ~240 mT); Lowrie's (1990) method indicates that ferrimagnetic minerals (the intermediate axis shows blocking temperatures ~400 and 550°) are also magnetic carriers in these samples (Fig. 5c). The NRM bulk intensities of the tuffs range between 0.002 and 0.005 A m^{-1} and their initial susceptibilities range between 5×10^{-6} SI and 20×10^{-6} SI.

We applied AF and thermal demagnetizations to the tuffs of the Los Colorados section and found different magnetic behaviors. Fig. 5d depicts samples in which the ChRMs were readily determined by applying the least-squares line fitting (MAD values $\leq 5°$) at steps greater than 500 °C. The ChRMs of these samples are directed upward with a medium inclination to the NNW, similar to those of the site formed by the basaltic lava flow and the peperite. In other samples, the data track along a great circle path, and their

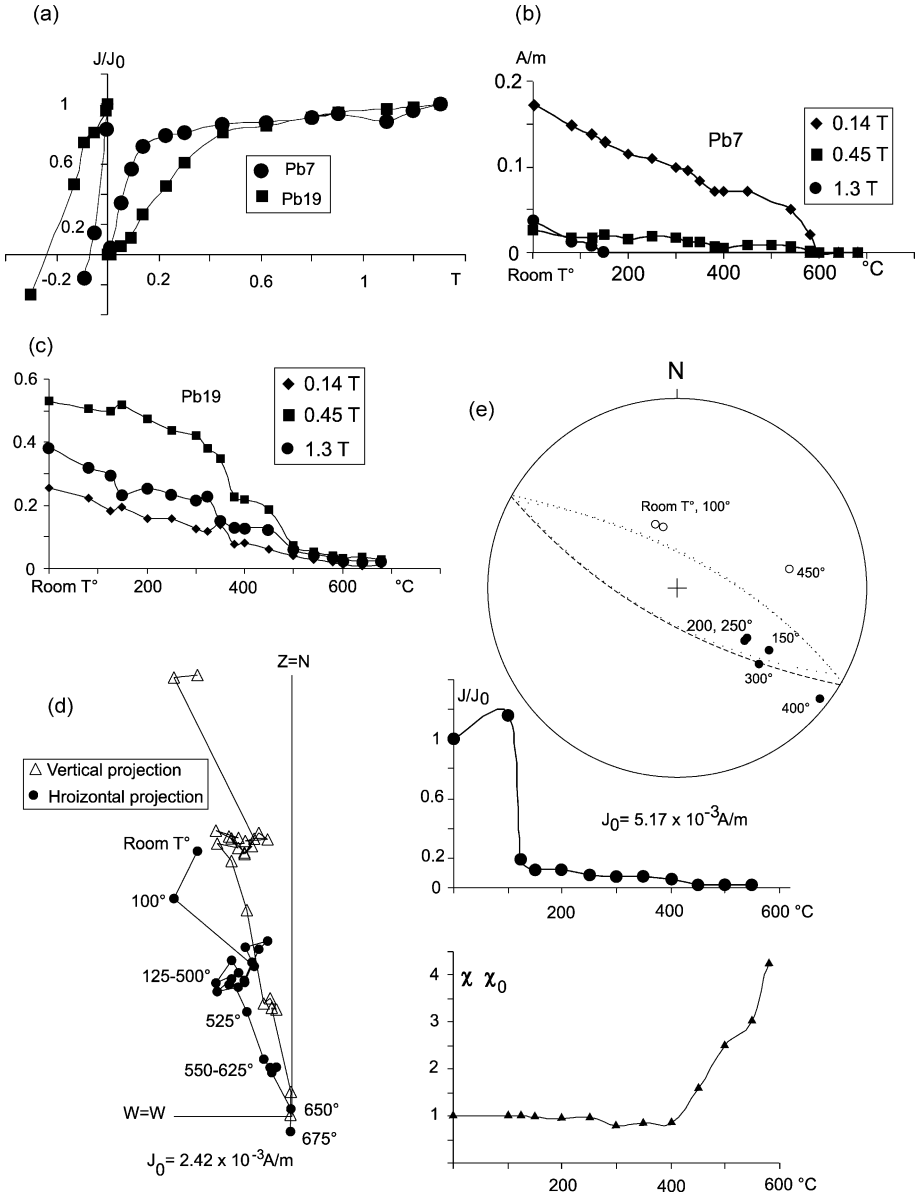

Fig. 5. Tuffs. (a) IRM acquisition curves and backfields of two representative samples (PB 7 and PB 18). (b and c) Thermal demagnetizations of three IRM of different forces applied successively to each of three perpendicular axes of the analyzed samples; (b) sample PB 7, (c) sample PB 18. (d) Orthogonal plot of thermal demagnetization of a representative sample; symbols and reference as in Fig. 2. (e) Stereonet plot of resultant vectors after thermal cleaning (symbols as in Fig. 4), normalized intensity decay (J/J_0) and bulk susceptibility evolution (χ/χ_0) after the applied steps of thermal demagnetization.

NRM is probably composed of two magnetic vectors (Fig. 5e). In the case of Fig. 5e, the data are randomly distributed after 400°. The sample loses its intensity and the susceptibility changes significantly at 450 °C. indicating that the NRM was completely lost because of the thermal generation of new magnetic minerals. The great circle paths in these samples could contain the direction determined by least-square fitting.

3.3. Complementary section

Three paleomagnetic sites were sampled in the complementary section. Two of the sites have the same bedding attitude and consist of a very fine-grained volcanic mudstone overlying and an altered vesicular olivine basalt. The site with a different bedding plane orientation is a fine-grained, laminated crystal-lithic tuff.

Olivine is extensively altered to limonite and haematite in the basalt and encloses several spinel phases including chromite, a pale brown? chrome-rich spinel, and magnetite. Chromite (5–60 μm diameter) is locally enclosed in magnetite rims, alters to ferrochromit, and is cut by thin, 1–2 μm wide haematite veinlets. Magnetite up to 100 μm in diameter is concentrated at the edges of olivine crystals. Locally, it forms clusters and is oxidized to maghaematite and to haematite. Within the groundmass ilmenite laths that

have been pseudomorphed by fine-grained haematite and TiO_2 are abundant; magnetite, as skeletal crystals, is oxidised to haematite, though some relict, unaltered magnetite remains as 10–20 μm diameter grains. The IRM acquisition (FT 6 in Fig. 6a) and backfield curves (H_{cr} of ~40 mT) show that a ferrimagnetic mineral (magnetite?) is the main carrier of the remanence, in agreement with the petrographic analysis. The NRM intensities are approximately 0.3 A m^{-1}, and its bulk initial susceptibilities range between 2000×10^{-6} SI and $10{,}000\times10^{-6}$ SI.

The very fine-grained volcanic mudstones overlying the basalt, carry abundant <1–2 μm long pigmentary haematite crystals that turn many of the clasts to be opaque. Haematite is also present as 10–60 μm diameter single crystals or fine-grained mosaics. The rocks also have 40 μm diameter chromite and a grey spinel with thin, 1–2 μm wide haematite rims, as well as mixed haematite–TiO_2 that replaces original iron–titanium oxides and martite that replaces original magnetite but with some relict magnetite. The IRM acquisition and backfield curves (FT 8 in Fig. 6a) show that haematite/goethite (H_{cr} of ~600 mT) is the main remanence carrier, which is consistent with the petrographic analysis. The NRM intensity of this rock is approximately 0.010 A m^{-1}, and its initial susceptibilities range between 100×10^{-6} SI and 200×10^{-6} SI.

The fine-grained laminated crystal–lithic tuffs carry abundant haematite pigment. Different spinels are present including 10–20 μm diameter, grey chromite that shows partial alteration to ferrochromit and haematite and a pale brown spinel that is altered to haematite. Magnetite, up to 20 μm in diameter, is altered to haematite/martite. Minor amounts of 20–40 μm long altered ilmenite and 10–20 μm diameter mixed haematite–TiO_2 that replaces original iron–titanium oxides are present. Rock magnetic parameters

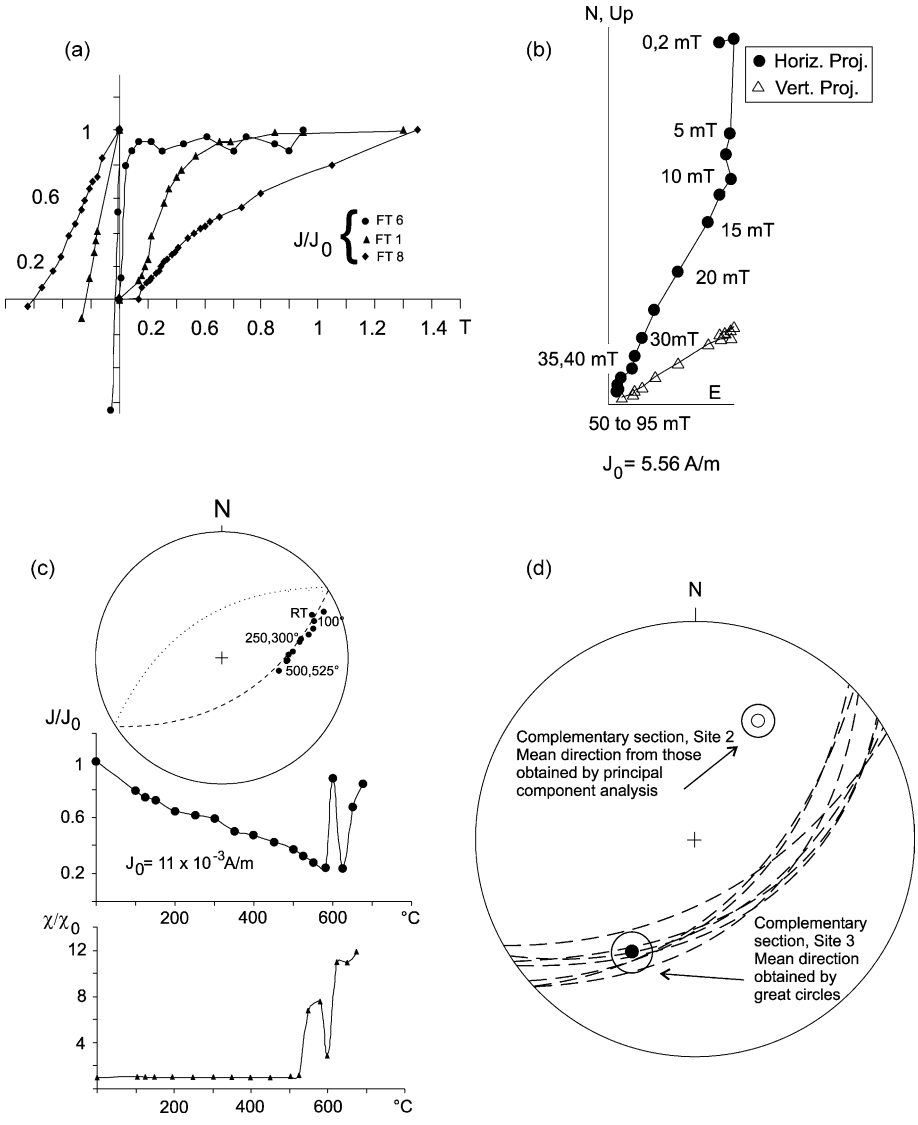

Fig. 6. Rocks of the complementary section. (a) IRM acquisition curves and backfield of representative samples. (b) Orthogonal plot of AF demagnetization of NRM of a representative sample; symbols and reference as in Fig. 2. (c) Orthogonal plot, stereonet plot, normalized intensity decay (J/J_0) and bulk susceptibility evolution (χ/χ_0) of a sample of the site C3 after thermal demagnetization. (d) Mean directions of sites C2 and C3 in geographic coordinates.

suggest ferrimagnetic and antiferromagnetic minerals, in agreement with the petrographic observations. Meanwhile, the IRM acquisition and backfield curves (FT1 in Fig. 6a) indicate haematite, the NRM bulk intensities range between 5 and 6 A m^{-1} and its initial susceptibility is approximately 6000×10^{-6} SI, in agreement with the ferrimagnetic minerals also observed by petrographic analysis.

Depending on the carriers of the remanences, thermal and AF demagnetization were applied to the basalt and crystal–lithic tuff, but only thermal cleaning was applied to the volcanic mudstone. In the samples of the crystal–lithic tuff and the basalt, very well-defined ChRMs (MAD values $\leq 5°$) were determined as shown in Fig. 6b. In this case, the sample has two components. A magnetically soft section was easily removed at approximately 10 mT and lies in the direction of the present-day dipolar geomagnetic field. The ChRM was defined at steps over 12 mT and is directed NNE with an intermediate upward inclination. The least square fitting method was not useful for the samples of the volcanic mudstone. The data from these samples track along a great circle path in the stereographic projection until 525 °C (Fig. 6c). After this demagnetization step, the data are not reliable and new magnetic minerals probably are generated, according to the changes in intensity and susceptibility. A direction antipodal to the mean direction of the basalt was obtained by applying McFadden and McElhinny (1988) method, using the seven great circles recognized in the samples of the volcanic mudstone (Fig. 6d).

3.4. Miocene rocks

To compare the magnetic components recorded in the Upper Triassic–Lower Jurassic rocks of the Los Colorados section, two paleomagnetic sites were sampled in the Miocene rocks in the upper part of the section. One of the sites is within the andesites of the Miocene volcano of Los Colorados hill, and the other is in the red beds that are interbedded with the Miocene andesites.

The IRM acquisition of the andesites (Fig. 7a) shows a sharp rise in $H<200$ mT followed by the gradual acquisition of additional IRM in stronger H. The backfield curve and AF demagnetization of IRM (Cisowski, 1981) show H_{cr} between 40 and 60 mT. According to these characteristics a ferrimagnetic mineral is the main magnetic carrier of the remanence. The blocking temperatures observed (Lowrie, 1990) indicate that magnetite (Fig. 7b) with subordinate haematite is the main remanence carrier. Magnetite (20–120 μm) with rims of haematite was petrographically recognized. The NRM bulk intensity is approximately 1 A m^{-1}, and its initial susceptibility is approximately 2600×10^{-6} SI. Thermal and AF demagnetizations and a mixed AF/thermal cleaning were applied to the specimens. Very well-defined ChRMs (MAD values $\leq 5°$) directed downward to the SE were determined in all the samples, and the in situ site mean direction was Dec. = 134.43°, Inc. = 47.89° ($N=4$, $\alpha_{95}=6.5°$, $K=202.8$).

The red beds interbedded with the andesites are immature arkosic sandstones. The IRM acquisition of these rocks (Fig. 8a) showed a sharp rise at $H<200$ mT and a magnetic saturation in low H. The backfield and the AF demagnetization of IRM indicate a H_{cr} of about 15 mT. These characteristics indicate that a ferrimagnetic mineral is the main carrier of the remanence. Petrographic observations permitted the identification of relict magnetite 20–60 μm in diameter and 5–60 μm areas of ilmenite, both with intense haematite–TiO_2 alteration. Magnetite grains are extensively altered to maghaematite, which is, itself altered to haematite or martite. Fine-grained TiO_2 minerals accompany this alteration. The NRM bulk intensities of the samples range between 0.02 and 0.03 A m^{-1}, and its initial susceptibility is 2000×10^{-6} SI (three orders higher than the initial susceptibility recognized in the Mesozoic red beds). We applied thermal

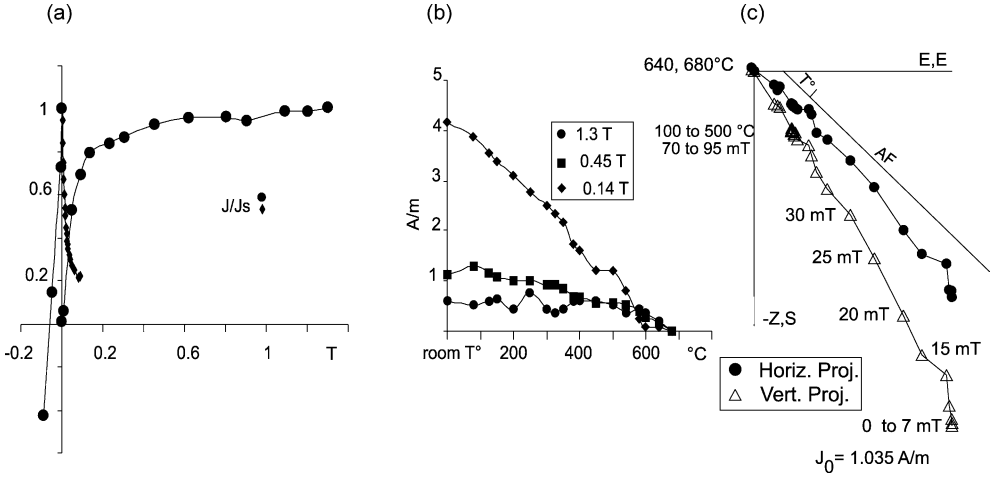

Fig. 7. Miocene andesite. (a) IRM acquisition curve, backfield and AF demagnetization of the saturation remanence of a representative sample. (b) Thermal demagnetizations of three IRM of different forces applied successively to each of three perpendicular axes of a representative sample. (c) Orthogonal plot of mixed AF/thermal demagnetization of NRM of a representative sample, symbols and reference as in Fig. 2.

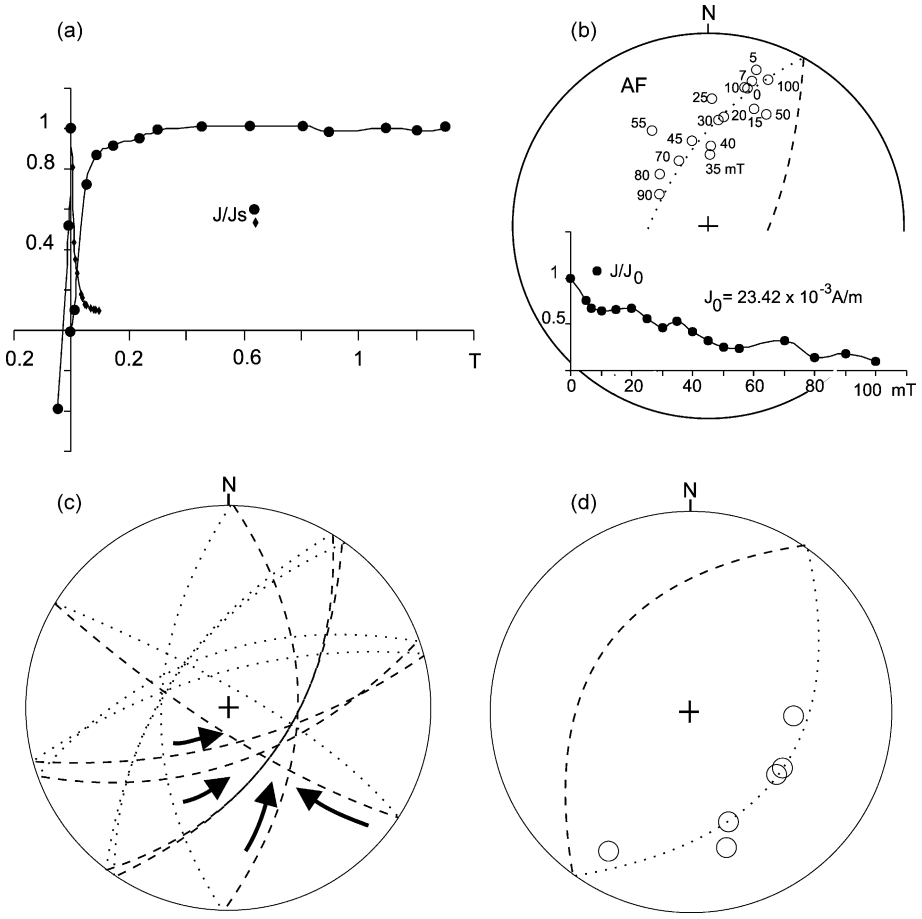

Fig. 8. Miocene sandstones. (a) IRM acquisition curve, backfield and AF demagnetization of the saturation remanence of a representative sample. (b) Stereonet plot of resultant vectors after AF demagnetization of a representative sample and normalized intensity decay of the same sample. (c) Stereonet showing remagnetization circles of six samples. (d) Remagnetization-circle normals and the great circle fitted to these normals, open circles are upward pointing.

and AF demagnetizations to the specimens, but the least square fitting method was not useful for defining the ChRMs. In the stereographic projection, the data track along great circles after the application of the successive demagnetization steps (Fig. 8b), and different great circles were determined for the different analyzed samples (Fig. 8c). To test if the great circles converge, we observe that the normals fall along a great circle fitted by least square (Fig. 8d) (Halls, 1978), for which the normal represents the estimate of the site direction. We used the McFadden and McElhinny (1988) method to define the site mean direction (in situ, Dec. = 126.36°, Inc. = 55.43°, $N = 6$, $\alpha_{95} = 9.4$, $K = 85.81$), which is similar to that determined in the interbedded andesites.

4. When was the direction in the great circles recorded?

As we have shown, two main types of magnetic behaviour occur in the Upper Triassic–Lower Jurassic rocks: Type 1, samples whose ChRMs can be defined using least square fitting, and Type 2, or multicomponent samples whose coercivity or blocking temperature spectra were overlapped. The ChRMs of Type 1 samples are directed upward with a moderate inclination. In Type 2 samples, a downwardly directed component is identified in the remagnetization circles.

There are sites in the Los Colorados section in which both types appear. Before combining the remagnetization circles and the ChRMs to obtain the mean directions of these sites, we investigated if the directions involved in the great circles are equivalent to those determined by applying least-squares line fitting.

4.1. Reversal test

We averaged the ChRMs from all samples of the Los Colorados section with Type 1 behaviour to obtain a mean direction (Dec. = 338.9, Inc. = −49.5, $N = 24$, $R = 23.18$, $\alpha_{95} = 5.7$, $K = 28$). We obtained another mean direction (Dec. = 155.25, Inc. = 59.1, $N = 30$, $R = 29.01$, $\alpha_{95} = 7.3$, $K = 14$) from the Type 2 samples using McFadden and McElhinny's (1988) method. To choose the polarity of the remanence, we took into account that, at the highest demagnetization temperature steps, the residual remanence moves toward a downward inclination. Both mean directions

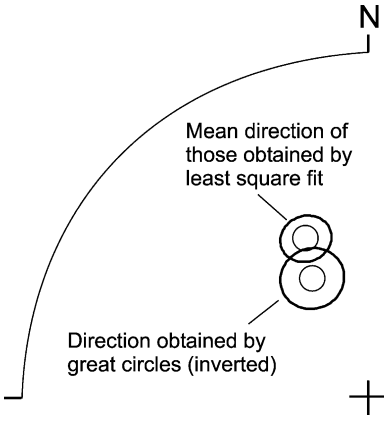

Fig. 9. Mean directions of Los Colorados section, obtained from the comparison of those determined by least square fitting with those determined using remagnetization circles.

are antipodal at 95% confidence (McFadden and Lowes, 1981) which indicates a positive reversal test (Fig. 9).

However, the latitudinal locations of South America have been similar from the Permian to the Present, and the rocks of this continent could have recorded similar geomagnetic fields directions at different geological ages. According to the geology of the area (see Section 2), an event that may have remagnetized the analyzed Upper Triassic–Lower Jurassic rocks is the magmatism that generated the Miocene volcano of Los Colorados hill (Fig. 1c). Therefore, using great circles, we compared the directions recorded by the Miocene rocks with those from the Mesozoic rocks.

4.2. Mean Miocene directions versus mean direction from great circle analyses of Upper Triassic–Lower Jurassic rocks

In Fig. 10a, we show the mean directions obtained from the great circle analyses for the Upper Triassic–Lower Jurassic red beds and tuffs of the Los Colorados section, the Miocene andesites, and the red beds that are interbedded with the andesites, as well as a Miocene reference direction for the sampling site (Randall, 1998). There is an overlap between the 95% confidence intervals of the Miocene directions, which implies that the direction of the volcano of Los Colorados hill is representative of the Miocene geomagnetic field. Both Miocene directions are close to that of the Upper Triassic–Lower Jurassic rocks, and there is a small overlap between the 95% confidence intervals of the directions that belong to the Miocene red beds and to the Upper Triassic–Lower Jurassic rocks. None of the in situ directions coincide with the Miocene reference direction.

Fig. 10b shows the same directions after the structural correction according to the bedding planes recognized in the Upper Triassic–Lower Jurassic rocks (strike 171°, inclination 21°). No reliable bedding planes were observed in the field for the Miocene rocks. As described in Section 2, the Miocene rocks overlie the Mesozoic with a very low-angle discordance. The Miocene directions are closer to the reference direction after the structural correction, and there are small overlaps between the 95% confidence intervals of the directions that belong to the Miocene rocks and the reference direction. Therefore, the structure of the Los Colorados section is probably younger than Miocene. There is also an overlap between the 95% confidence intervals of the directions of the Upper Triassic–Lower Jurassic rocks and the Miocene reference direction. The mean direction of the Mesozoic rocks therefore could be a remagnetization recorded before the tectonic deformation of the studied section. According to this analysis, a ‘fold test’ is not enough to demonstrate that the directions of the Upper Triassic–Lower Jurassic rocks are primary; it is also necessary to prove that the mean direction of the great circles was not recorded during the magmatic event that generated the Miocene volcano.

4.3. Conglomerate test

We applied the conglomerate test proposed by Shipunov et al. (1998) to determine if unit vectors tend to cluster around a given direction—here, the mean direction of the Miocene andesites of the volcano. In the other tests, if an intraformational conglomerate is studied, the test constitutes virtually unequivocal proof that the remanence is primary. However, this rule may not hold for our study because the 29 analyzed clasts consist of acid ignimbrites and the host

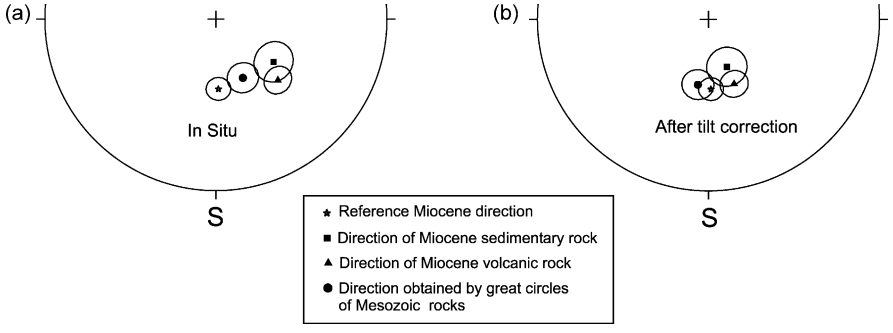

Fig. 10. Comparison between the mean direction obtained using circles of remagnetiztion circles (Upper Triassic–Lower Jurassic rocks) and Miocene directions, before and after tilt correction.

rocks are two conglomerates interbedded with the red beds of the Los Colorados section.

The acquisition of IRM, the backfield and the blocking temperatures of the clasts indicate that a ferrimagnetic mineral (magnetite?) and haematite are the main carriers of the remanences. We observed two different behaviours in the clasts after several steps of demagnetization. Fig. 11a shows an example in which only one magnetic vector was determined using the least square fitting method, whereas Fig. 11b is an example of a multicomponent clast. There is no overlap between the blocking temperatures of the different components, and the least square fitting method was used to define the softer and harder components. In Fig. 11c and d, both the softer and the harder components (including the monocomponent clasts) are represented together with the direction of the Miocene volcano. In both cases, Shipunov et al.'s (1998) test is positive, and the Miocene direction was not recorded by the clasts. However, this is less reliable here than in the case of an intraformational conglomerate, because the results of the clasts of one lithology are transferred to the results from the host rocks of a different composition. For that reason, we performed another test.

4.4. Change of the magnetic minerals of the basalt and peperite during heating and magnetic direction of the Miocene volcano

The Upper Triassic–Lower Jurassic basaltic lava flow and its associated peperite in the Los Colorados section lie closest to the Miocene andesites of the volcano (Fig. 1c). The samples of the basalt and peperite show a dominant component with upward inclination (normal polarity) opposite to the direction of the Miocene andesites (reverse polarity). However, significant changes in the susceptibility appear after the thermal heating of the basalt and peperite (Figs. 2d and 3d). We applied another methodology to confirm whether these changes in susceptibility belong to the generation of new magnetic minerals. The remanent

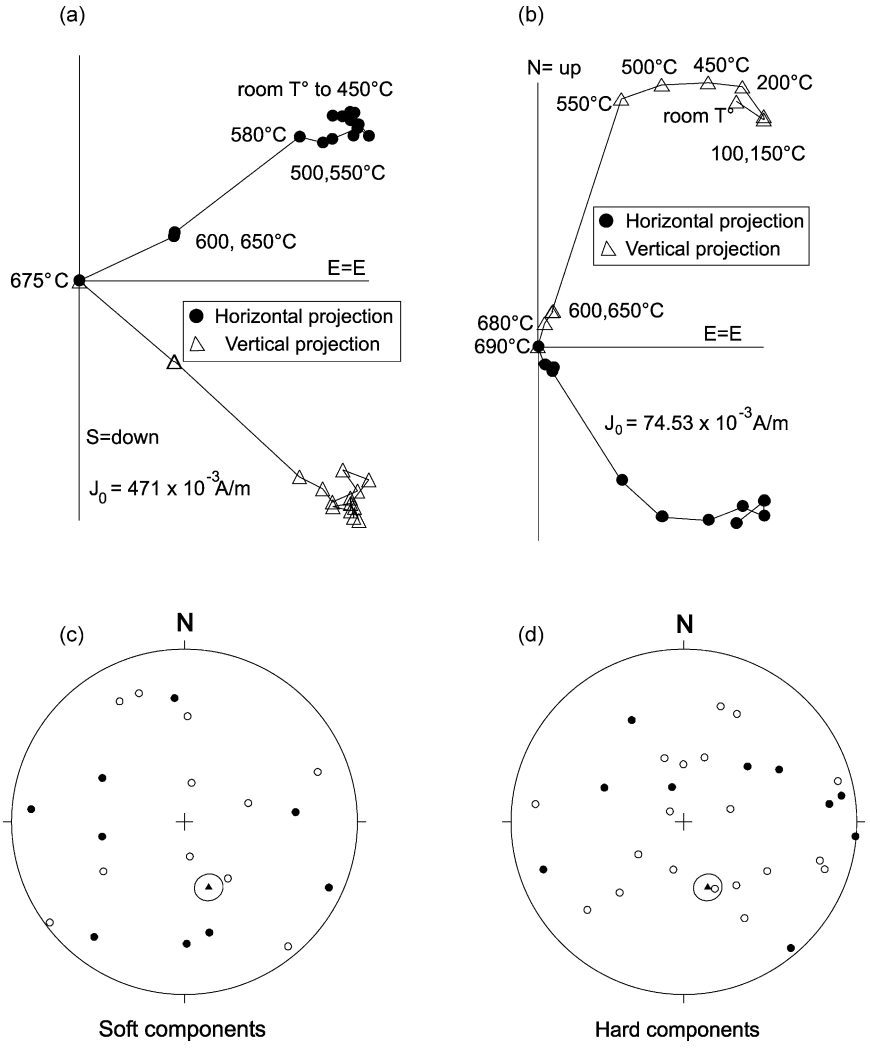

Fig. 11. Clasts of conglomerates. (a and b) Orthogonal plots of thermal demagnetization of the NRM of two different clasts. (a) Monocomponent, (b) multicomponent, (c and d) stereonets showing the softer and harder components determined in the clasts, the direction of the Miocene andesite is also shown with its 95% confidence interval.

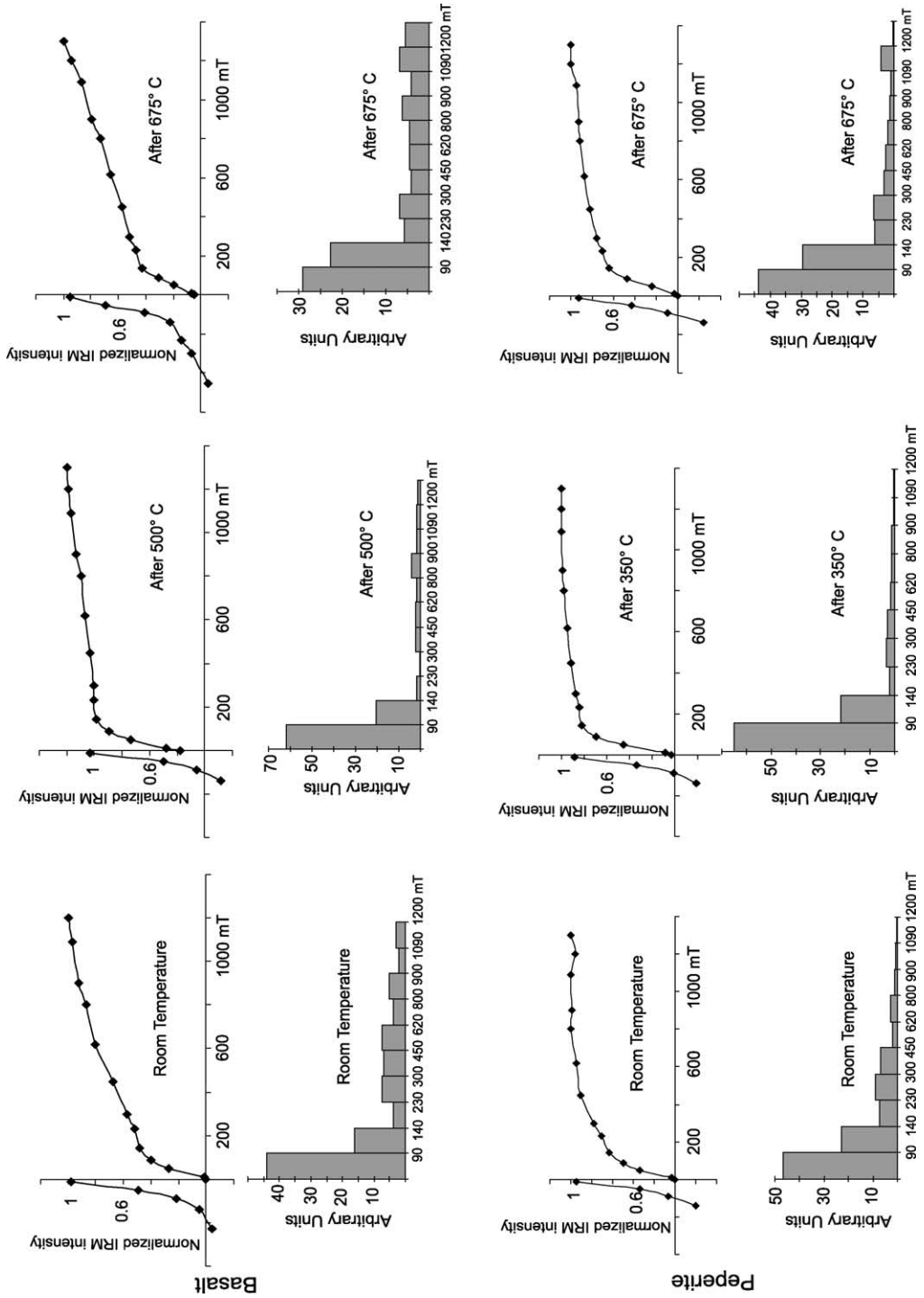

Fig. 12. Evolution of the coercivity spectra of the basaltic lava flow and its peperite when heated in air.

coercivity spectra derived from the IRM acquired after the application of successive steps of H (Dunlop, 1972) were determined for specimens of the basalt and the peperite (Fig. 12).

Experimentally, the samples were subjected to two heating steps selected on the basis of the changes observed in their susceptibilities. The IRM curves were determined by applying stepwise values of H with fresh samples each time at room temperature, after 500 or 350 °C and after 675 °C. The coercivity spectra were analyzed rather arbitrarily into their soft ($0 \leq H_{cr} \leq 90$ mT), intermediate (90 mT $\leq H_{cr} \leq 300$ mT), and hard (300 mT $\leq H_{cr} \leq 1200$ - mT) fractions. For the basalt, heating in air to 500 °C produces approximately 15% of the soft fraction, but heating to 675 °C reduces this fraction approximately 10% with respect to the first heating and increases the hard fraction (see the backfield curve). Thin section petrography reveals that limonite is lost after heating to 500 and 675 °C, and olivine is replaced by haematite at 675 °C. For the peperite, heating to 350 °C increases the soft fraction to 20%, but heating to 675 °C reduces this fraction 20% and increases the intermediate fraction with respect to the previous heating. The analyses confirm the generation of new magnetic minerals at different steps of thermal heating. If the magnetic event of the Miocene volcano had affected the basalt and peperite thermally, new magnetic minerals would have recorded the reverse polarity direction found in the Miocene andesites, Therefore, the basalt and peperite were not affected by the heating of the Miocene magmatic event, and because these rocks are closest to the volcano, it is likely that the rest of the lithologies of Los Colorados section were not affected either. The petrographic analysis of the red beds and tuffs of this section does not reveal evidence of metamorphism or hydrothermal alteration, and it seems likely that the remanences of these rocks are older than the magmatic event that generated the volcano.

4.5. Site mean directions and fold test

According to our tests, the directions involved in the great circle paths are not remagnetizations recorded during the Miocene. Assuming that these directions belong to the same geomagnetic field that generated those obtained by the least square fitting method, we can obtain site mean directions using McFadden and McElhinny's (1988) method, which combines remagnetization circles with ChRMs. These directions, together with those obtained using Fisher's (1953) method, are reported in Table 1. Fig. 13a and b shows all the Triassic–Jurassic directions before and after the structural correction and indicate that they pass the fold test (McFadden, 1990). To perform the structural corrections, we first restored the axis of the brachisyncline to the horizontal, correcting the site, the site mean directions and the strikes and dips. After that, the beds were unfolded using the corrected strikes and dips.

5. Discussion and conclusions

The sedimentary rocks in the Los Colorados section show sites with ChRMs with upward inclinations along and great circle paths that involve antipodal directions with downward inclinations. In these sites the remanences probably were recorded during at least two chrons of different magnetic polarities, though the age of both polarity components could be close to the stratigraphical age of the analyzed sequence. When the mean directions of the volcanic sites (S1 and C2) are compared with the mean directions of the sedimentary rocks after tilt corrections using McFadden's (1990) method, they share a common mean at the 95% confidence level. Assuming that the ages of the magnetic directions of both Los Colorados and the complementary sections are close to the ages of the rocks, We call this PP Rio Blanco (RB), and its

Table 1
Site characteristics

Site	N/No	Dec.g (°)	Inc.g (°)	K	α_{95}	Dec.h (°)	Inc.h (°)
S1	13/13	344.2	−47.1	40.9	6.6	5.0	−45.5
S2[a]	7/7	329.5	−47.5	16.2	16.9	352.5	−54.0
S3	4/6	340.7	−49.6	75.6	10.6	4.0	−48.8
S4[a]	4/4	308.3	−63.7	10.5	25.3	356.5	−70.8
S5[a]	7/8	334.2	−48.9	31.3	10.9	357.9	−50.5
S6[a]	6/10	320.3	−67.7	24.7	19.5	14.4	−68.9
S7[a]	5/6	330.3	−53.6	19.6	18.3	358.9	−55.7
S8[a]	4/6	328.6	−68.8	19.9	28.6	21.1	−66.9
S9[a]	4/8	314.3	−65.0	45.6	14.2	4.3	−69.5
C1	3/4	22.8	−13.9	2401.5	2.5	328.1	−59.3
C2	8/8	28.7	−27.9	75.4	6.4	353.8	−55.5
C3[a]	7/7	28.3	−28.4	91.7	7.7	352.7	−55.6

Notes: N(No) is the number of samples used (demagnetized) in mean calculations. Dec.g and Inc.g are declination and inclination in geographic coordinates. Dec.h and Inc.h are declination and inclination in the paleohorizontal after the structural correction. The statistical parameters K and α_{95} are Fisher's precision parameter and the radius of the 95% cone of confidence. To perform the structural corrections: Axis of the braquisyncline, northern sector: plunge 9° to the south (Azimuth 198°), southern sector: plunge 10° to the north (Azimuth 351°). For sites S, strike: 171°, Inc.: 21° (N=7, α_{95}=5.4°, K: 124.87, R=6.95). For site C1, strike: 324°, Inc.: 68°. For site C2 and C3, strike: 335°, Inc.: 42°.

[a] Sites include samples with great circles of remagnetization that would involve a positive component.

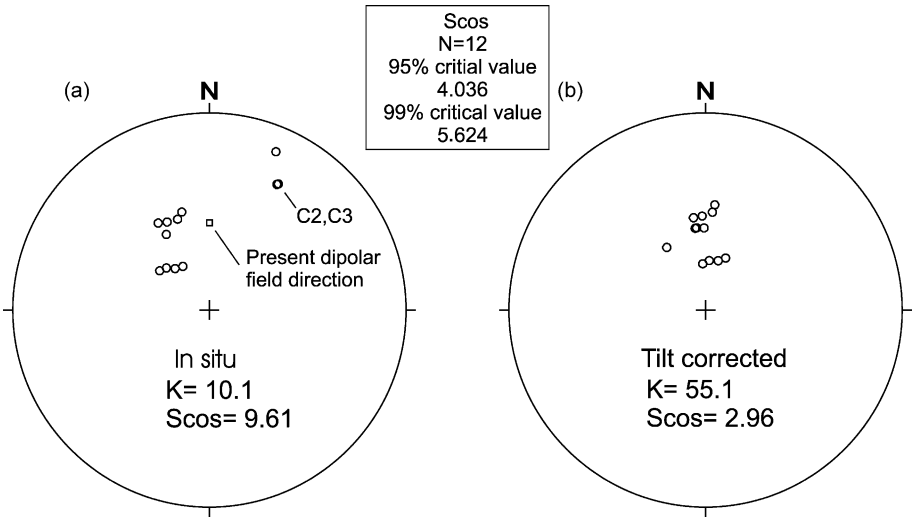

Fig. 13. Site mean directions of the Upper Triassic–Lower Jurassic rocks. (a) In situ. (b) After tectonic correction. The statistical parameters of the 'fold test' of McFadden (1990) are also shown.

geographic coordinates and statistical parameters are as follows: Lat.=81.8°S, Long.=298.3°E, $N=12$, $R=11.7$, $\alpha_{95}=7.6°$, $K=33.9$.

According to the stratigraphical information in Section 2, the sampled rocks are late Middle Triassic to Latest Triassic or even Early Jurassic (Hettangian). This time-span covers Late Triassic ages with chronological limits between 227.4 and 205.7 Ma according to Gradstein et al. (1994), or between 230 and 203 Ma according to the International Union of Geological Sciences (2000).

We compared the RB with Triassic PPs of South America (Table 2, Fig. 14a). The selected PPs have quality factors $Q\geq 3$ (Van der Voo, 1993). However, this comparison is only tentative because, as we mentioned in Section 1, the Triassic PPs of South America were obtained using old methodologies, and their ages must be updated. The PP RB forms part of the population of the selected PPs (isolated test, McFadden, 1990).

We also performed a comparison with two selected PPs of Africa with $Q\geq 3$ (Fig. 14b and Table 2). We used the finite pole of rotation (Nürnberg and Müller, 1991; Lat.=50.0°N, Lon.=32.5°W, rotation angle=55.08°) was used to transfer RB to African geographic coordinates and closed the Paraná basin with the finite pole of rotation (Lat.=15.2°S, Lon.=73.2°W, rotation angle=1.48°). After this rotation, there is a very good fit between the South American and African PPs (Fig. 14b).

Finally, we compared RB with paleomagnetic data from Laurasia. Mean PPs that belong to the time-span between 250 and 200 Ma North America geographic coordinates were taken from Table 2 of Torsvik et al. (2001). To perform this comparison, we transferred the data from Laurasia to African geographic coordinates using the finite pole of rotation of Klitgord and Schouten (1986; Lat.=67°N, Lon.=347.7°E, rotation angle=75.5°), which belongs to a model of Pangea A. In Fig. 15a, we show

Table 2
Selected Triassic Paleomagnetic poles

Geological unit	Longitude	Latitude	α_{95} or $\delta p+\delta m$	Geological age	References
South America					
Guyana Dikes (GY)	208.9	−63.8	10.5	Early Trias.	Hargraves (1975)
Amaná Fm. (AM)	317.0	−83.0	8	Early Trias.	Valencio et al. (1977)
Talampaya Fm. (TL)	177.9	−78.9	9	Early Trias.	Valencio et al. (1977)
El Nihuil Lavas (NI)	282.0	−81.0	6	Early Trias.	Creer et al. (1970)
Surinam Dikes (SU)	320.0	−82.0	15	Mid. Trias.	Veldkamp et al. (1971)
Cuesta Terneros (CT)	228.0	−80.0	10	Mid. Trias.	Creer et al. (1970)
Puesto Viejo Fm. (PV)	230.8	−75.3	15.5	Mid. Trias.	Valencio et al. (1975)
Cacheuta Basalts (CH)	266.0	−74.0	14.5	Late Trias.	Valencio (1969)
Ischigualasto Lavas (IS)	239.2	−79.2	15	Late Trias.	Valencio et al. (1975)
Río Blanco Fm. (RB)	298.3	−81.8	7.6	Late Trias.	This study
Africa					
Cassanje Series (CA)	254.00	61.00	8	Mid. Trias.	Valencio et al. (1978)
Argana Red beds (AR)	251.00	51.00	12	Late Trias.	Martin et al. (1978)

Notes: α_{95} radius of the 95% cone of confidence, $\delta p+\delta m$ are the axes of the 95% ellipse of confidence.

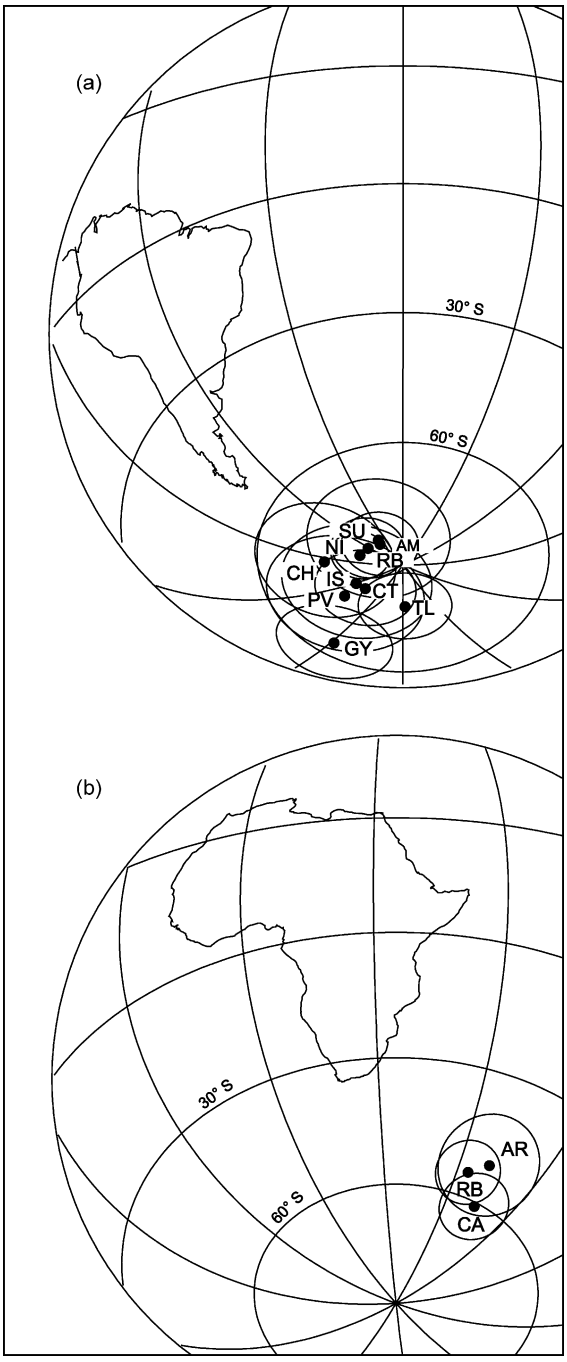

Fig. 14. (a) Triassic PPes PPs of South America including RB PP (Table 2) in South American geographic coordinates. (b) Triassic PPs of Africa and RB PP transferred to African geographic coordinates.

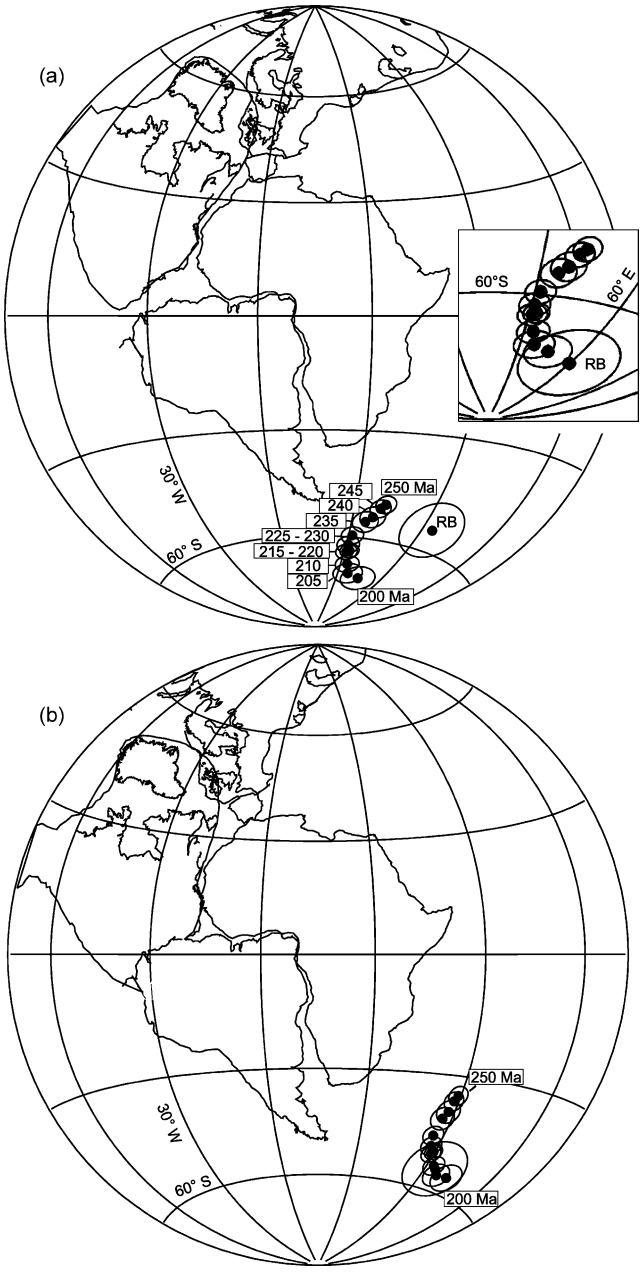

Fig. 15. Laurasia apparent polar wander path (Torsvik et al., 2001) and RB PP in African geographic coordinates. (a) According to a model of Pangea A, inset: after a rotation of the sampling area around a vertical axis. (b) According to a model of Pangea A_2 (see text for further explanation).

that RB does not fit with any data from Laurasia, which could be due to at least two different tectonic reasons.

Our first interpretation involves local tectonics that could have undergone a counterclockwise rotation of the sampling area around a vertical axis. Note that the 95% circle of confidence of RB overlaps the PPs of 205 and 200 Ma after a clockwise rotation of 25° using a finite pole of rotation in the sampling area (Fig. 15a inset). According to our paleomagnetic data, a counterclockwise rotation around a vertical axis of the sampling locality should have occurred before the Miocene. A generalized extensional regime continued in the intracratonic region during most of the Jurassic and Early Cretaceous (Kokogian and Mancilla, 1989; Ramos and Kay, 1991), which reactivated the NW Triassic rifts. Large NNE-trending faults in the rift could have been reactivated by left-lateral strike–slip, arranged the extensional deformation, and rotated different blocks counterclocwise, including our sampling locality.

The second interpretation involves global tectonics. For this case, we compared the data with a model of Pangea A2

and rotated the Laurasia PPs using the finite pole of rotation proposed by Van der Voo and French (1974; Lat. = 19.3°N, Lon. = 0.69°W, with a counterclockwise rotation of Laurasia of 20° respect to Gondwana). There is an excellent fit between RB and Late Triassic PPs of Laurasia (Fig. 15a). The agreement between the PPs of the different continents in this reconstruction is in accordance with a Pangea A2 model that is very well supported both geologically and tectonically for the Late Triassic (Golonka et al., 1994). The model of Pangea B is not as well supported geologically. There is consensus that the Atlantic Ocean opened from a Pangea A configuration. If Pangea B existed previously, a transition to Pangea A would require a large (~3500 km) dextral megashear between the northern and southern continents which is not well supported in terms of the geology of the Gondwana–Laurasia border zone (i.e. Hallam, 1983). Therefore, we did not compare with PPs of Laurasia in a Pangea B model.

Both interpretations performed with models of Pangea A, were carried out with only one PP from Gondwana, so the conclusions are not definitive. Nonetheless, some speculations can be made about the position of RB with respect to the data from Laurasia. In both cases, it is not necessary to invoke a model of non-dipolar geomagnetic field for the Late Triassic, as suggested by Van der Voo and Torsvik (2001) for the Late Paleozoic–Early Mesozoic. Two possibilities can be considered in agreement with this: the time-averaged paleomagnetic field was non-dipolar for times older than Late Triassic, or it was dipolar from times older than Late Triassic and the apparent non-dipolar behaviour is the result of data with different problems (e.g. remagnetizations, poor structural corrections, erroneous age determinations).

Acknowledgements

We thank the Universidad de Buenos Aires, the University of Birmingham and CONICET (Consejo Nacional de Investigaciones Científicas y Técnicas) for financial support of the research. Dr J. Genise helped us during the fieldwork. Special thanks to Drs R. Somoza, S.E. Geuna, C. Marcicano (U.B.A.) for help with a revision of a prevous version of this paper. H.V. is in debt to the research staff of the 'old' School of Earth Sciences of the University of Birmingham. The careful reviews by Drs D. Tarling and A. Rapalini, are appreciated.

References

Artabe, A.E., Brea, M., Zamuner, A.B., 1999. *Rhexoxylon brunoi* Artabe Brea et Zamuner, sp. Nov., a new Triassic Corystosperm from the Paramillo de Uspallata, Mendoza, Argentina. Review of Palaeobotany and Palynology 105, 63–74.

Arthaud, F., Matte, P., 1977. Late Paleozoic strike–slip faulting in southern Europe and northern Africa: result of a right-lateral shear zone between the Appalachians and the Urals. Geological Society of America Bulletin 88, 1305–1320.

Briden, J.C., Smith, A.G., Sallomy, J.T., 1970. The geomagnetic field in Permo-Triassic time. Geophysical Journal of the Royal Astronomical Society 23, 101–117.

Busby-Spera, C.J., White, J.D.L., 1987. Variation in peperite textures associated with different host-sediment properties. Bulletin of Volcanology 49, 765–775.

Cisowski, S., 1981. Interacting vs. non-interacting single domain behavior in natural and synthetic samples. Physics of the Earth and Planetary Interiors 26, 56–62.

Cortés, J.M., González Bonorino, G., Koukharsky, M.L., Pereyra, F.X., Brodtkorb, A., 1997. Hoja 3369-09, Uspallata, Provincia de Mendoza. In Subsecretaría de Minería de la Nación, Servicio Geológico Minero Argentino.

Creer, K.M., Embleton, B.J., Valencio, D.A., 1970. Triassic and Permo-Triassic paleomagnetic data for South America. Earth and Planetary Science Letters 8, 173–178.

Dunlop, D.J., 1972. Magnetic mineralogy of unheated and heated red sediments by coercivity spectrum analysis. Geophysical Journal of Astronomical Society 27, 37–55.

Fisher, R.A., 1953. Dispersion on a sphere. Proceedings of the Royal Society of London, Series A 217, 295–305.

Fossa-Mancini, E., 1937. Las investigaciones geológicas de Y.P.F. en la provincia de Mendoza y algunos problemas de estratigrafía regional. Boletín de Informaciones Petroleras 14 (154), 51–118.

Geuna, S.E., Ecostegui, L., 2003. Palaeomagnetism of upper Carboriferous-lower permian transition from paganzo basin, Argentina. Geophysical Journal International 157, 1071–1089.

Golonka, J., Ross, M.I., Scotese, C., 1994. Phanerozoic paleogeographic and paleoclimatic modeling maps. In: Embry, A.F., Beauchamp, B., Glass, D.J. (Eds.), Pangea: Global Environments and Resources Canadian Society of Petroleum Geologist, Memoir, 17, pp. 1–48.

Gradstein, F.M., Agterberg, F.P., Ogg, J.G., Hardenbol, J., Veen, P. van, Tierry, M., Huang, Z., 1994. A Mesozoic time scale. Journal of Geophysical Research 99 (B12), 24051–24074.

Hallam, A., 1983. Supposed Permo-Triassic megashear between Laurasia and Gondwana. Nature 301, 499–502.

Halls, H.C., 1978. The use of converging remagnetization circles in palaeomagnetism. Physics of the Earth and Planetary Interiors 16, 1–11.

Hargraves, R.B., 1975. Problems in Paleomagnetic synthesis illustrated by results from Permo-Triassic dolerites in Guyana. Physics of the Earth and Planetary Interiors 16, 277–284.

Harrington, H.J., 1971. Descripción geológica de la Hoja 22c, Ramblón, Provincias de Mendoza y San Juan. Dirección Nacional de Geología y Minería, Boletín 114, 81pp.

Hoffman, K.A., Day, R., 1978. Separation of multicomponent NRM: a general method. Earth and Planetary Science Letters 40, 433–438.

International Union of Geological Sciences, 2000. International Stratigraphic Chart. Compiled by J. Remane, A. Faure-Muret, G.S. Odin. In: Remane, J., Cita, M.B., Dercourt, J., Bouysse, P., Repetto, F.L., Faure-Muret, A. (Eds.), Courtesy of the Division of Earth Sciences. UNESCO, Secretariat at Geological Survey of Norway, Trondheim, Norway.

Irving, E., 1977. Drift of the major continents since the Devonian. Nature 270, 304–309.

Kent, D.V., Olsen, P.E., 2000. Magnetic polarity stratigraphy and paleolatitude of the Triassic–Jurassic Blomidon Formation in the Fundy basin (Canada): implications for early Mesozoic tropical climate gradients. Earth and Planetary Science Letters 179, 311–324.

Kirschink, J., 1980. The least-squares line and plane and the analysis of palaeomagnetic data. Geophysical Journal of the Royal Astronomical Society 62, 699–718.

Klitgord, K.D., Schouten, H., 1986. Plate kinematics of the central Atlantic, In: Vogt, P.R., Tucholke, H. (Eds.), The Geology of North America The Western North Atlantic Region, vol. M. Geological Society of America, New York, pp. 351–378.

Kokogian, D., Boggetti, D., 1987. Reconocimiento de las formaciones Barrancas y Punta de las Bardas en la zona de Paramillos de Uspallata, Prov. Mendoza, Argentina. 10° Congreso Geológico Argentino, Actas III, 131–134.

Kokogian, D.A., Mancilla, O., 1989. Análisis estratigráfico secuencial de la Cuenca Cuyana. In: Chebli, G.A., Spalletti, L.A. (Eds.), Cuencas Sedimentarias Argentinas Universidad Nacional de Tucumán, Serie Correlación Geológica, 6, pp. 169–201.

Kokogian, D.A., Fernández Seveso, F., Mosquera, A., 1993. Las secuencias sedimentarias triásicas. In: Ramos, V.A. (Ed.), Geología y Recursos Naturales de Mendoza Relatorio 12° Congreso Geológico Argentino y 2° Congreso de Exploración de Hidrocarburos, pp. 65–78.

Kokogian, D., Spalletti, L.A., Morel, E.M., Artabe, A.E., Martínez, R.N., Alcober, O.A., Milana, J.P., Zavattieri, A.M., Papú, O.H., 2000. Los depósitos continentales triásicos. In: Caminos, R., Panza, J. (Eds.), Geología de la República Argentina Instituto de Geología y Recursos Minerales, Anales, 29(15), pp. 377–398.

Lowrie, W., 1990. Identification of ferromagnetic minerals in a rock by coercivity and unblocking temperature properties. Geophysical Research Letters 17 (2), 159–162.

Martin, D.L., Nairn, A.E.M., Noltimier, H.C., Petty, M.H., Schmitt, T.J., 1978. Paleozoic and Mesozoic paleomagnetic results from Morocco. Tectonophysics 44, 91–114.

Massabie, A.M., Rapalini, A.E., Soto, J.L., 1985. Estratigrafía del cerro Los Colorados, Paramillos de Uspallata, Mendoza. 1as Jornadas sobre Geología de Precordillera, Acta I, 71–76.

McFadden, P.L., 1990. A new fold test for palaeomagnetic studies. Geophysical Journal International 103, 163–169.

McFadden, P.L., Lowes, F.J., 1981. The discrimination of mean directions drawn from Fisher distributions. Geophysical Journal of the Royal Astronomical Society 67, 19–33.

McFadden, P.L., McElhinny, M.W., 1988. The combined analysis of remagnetization circle and direct observation in paleomagnetism. Earth and Planetary Science Letters 87, 161–172.

Muttoni, G., Kent, D.V., Channell, J.E.T., 1996. Evolution of Pangea: paleomagnetic constraints from the Southern Alps, Italy. Earth and Planetary Science Letters 140, 97–112.

Nürnberg, D., Müller, R.D., 1991. The tectonic evolution of the South Atlantic from Late Jurassic to Present. Tectonophysics 191, 27–53.

Ramos, V.A., Kay, S.M., 1991. Triassic rifting and associated basalts in the Cuyo basin, central Argentina. In: Harmon, R.S., Rapela, C.W. (Eds.), Andean Magmatism and its Tectonic Setting Geological Society of America, Special Paper 265, Boulder, pp. 79–91.

Randall, D.E., 1998. A new Jurassic-Recent apparent polar wander path for South America and a review of central Andean tectonic models. Tectonophysics 299 (1–3), 49–74.

Ricou, L.E., 1994. Tethys reconstructed: plates, continental fragments and their boundaries since 260 Ma from Central America to South-eastern Asia. Geodynamica Acta 7 (4), 169–218.

Rochette, P., Vandamme, D., 2001. Pangea B: an artifact of incorrect paleomagnetic assumptions? Annali di Geofisica 44 (3), 649–658.

Rolleri, E.O., Criado Roqué, P., 1968. La cuenca triásica del norte de Mendoza. Actas 3a Jornadas Geológicas Argentinas 1, 1–76.

Shipunov, S.V., Muraviev, A.A., Bazhenov, M.L., 1998. A new conglomerate test in paleomagnetism. Geophysical Journal International 133 (3), 721–725.

Smith, A.G., 1997. Estimates of the Earth's spin (geographic) axis relative to Gondwana from glacial sediments and paleomagnetism. Earth Science Reviews 42, 161–179.

Smith, A.G., 1999. Gondwana: its shape, size and position from Cambrian to Triassic times. Journal of African Earth Sciences 28 (1), 71–97.

Smith, A.G., Livermore, R.A., 1991. Pangea in Permian to Jurassic time. Tectonophysics 187, 135–179.

Smith, A.G., Hurley, A.M., Briden, J.C., 1981. Phanerozoic Paleocontinental World Maps. Cambridge University Press, Cambridge. 102 pp.

Spalletti, L.A., Artabe, A.E., Morel, E.M., Brea, M., 1999. Biozonación paleoflorística y cronoestratigrafía del Triásico Argentino. Ameghiniana 36 (4), 419–451.

Stipanicic, P.N., 1969. Las sucesiones triásicas argentinas. In: Amos, A.J. (Ed.), 1 Simposio Internacional sobre Estratigrafía y Paleontología del Gondwana, Mar del Plata Ciencias de la Tierra, 2. UNESCO, Paris, pp. 1121–1149.

Stipanicic, P.N., 1983. The Triassic of Argentina and Chile. In: Moullade, M., Nairn, A.E.M. (Eds.), The Phanerozoic Geology of the World, 2 The Mesozoic, B, 7. Elsevier, Amsterdam, pp. 181–199.

Strelkov, E., Alvarez, L., 1984. Análisis estratigráfico y evolutivo de la cuenca triásica mendocina-sanjuanina. Actas 9° Congreso Geológico Argentino 3, 115–130.

Torcq, F., Besse, J., Vaslet, D., Marcoux, J., Ricou, L.E., Halawani, M., Basahel, M., 1997. Paleomagnetic results from Saudi Arabia and the Permo-Triassic Pangea configuration. Earth and Planetary Science Letters 148, 553–567.

Torsvik, T.H., Van der Voo, R., Meert, J.G., Mosar, J., Walderhaugh, H.J., 2001. Reconstructions of the continents around the North Atlantic at about the 60th parallel. Earth and Planetary Science Letters 187, 55–69.

Valencio, D.A., 1969. El paleomagnetismo de algunas magmatitas del Triásico Superior, Grupo Cacheuta. Provincia de Mendoza, República Argentina. Revista de la Asociación Geológica Argentina 24 (3), 191–198.

Valencio, D.A., 1980. El magnetismo de las rocas. In Editorial Universitaria de Buenos Aires, Buenos Aires.

Valencio, D.A., Mendía, J., Vilas, J.F., 1975. Paleomagnetism and K/Ar ages of Triassic igneous rocks from the Ischigualast–Ischichuca basin and Puesto Viejo Formation, Argentina. Earth and Planetary Science Letters 26 (3), 319–330.

Valencio, D.A., Vilas, J.F., Mendía, J.E., 1977. Paleomagnetism of a sequence of red beds of the middle and upper sections of Paganzo Group (Argentina) and the correlation of upper Paleozoic–lower Mesozoic rocks. Geophysical Journal of the Royal Astronomical Society 62, 27–39.

Valencio, D.A., Rocha-Campos, A.C., Pacca, I.G., 19788. Paleomagnetis of the Cassange Series (Karroo System), Angola. Anais da Academia Brasileira de ciencias, 50: 353–364.

Van der Voo, R., 1993. Palaeomagnetism of the Atlantic, Tethys and Iapetus Oceans. Cambridge University Press, Cambridge.

Van der Voo, R., French, R.B., 1974. Apparent polar wandering for the Atlantic-bordering continents: Late Carboniferous to Eocene. Earth-Science Reviews 10, 99–119.

Van der Voo, R., Torsvik, T.H., 2001. Evidence for late Paleozoic and Mesozoic non-dipole fields provides an explanation for the Pangea reconstruction problems. Earth and Planetary Science Letters 187, 71–81.

Veldkamp, J., Mulder, F.G., Zijderveld, J.D.A., 1971. Paleomagnetism of Surinam dolerites. Physics of the Earth and Planetary Interiors 4, 370–380.